AIAA JOURNAL
Vol. 42, No. 7, July 2004

Buckling Response of Transversely Loaded Composite Shells, Part 1: Experiments

Mark A. Tudela,* Paul A. Lagace,† and Brian L. Wardle‡
Massachusetts Institute of Technology, Cambridge, Massachusetts 02139

The transverse loading response of convex composite shell structures typical of aircraft fuselage sections was investigated, and the experimental work is reported. Important mechanisms in the response, particularly instabilities (buckling), were studied by investigation of the force-deflection response and the evolution of full-field deformation shapes. Quasi-static tests were conducted to simulate impact of convex shells. The specimens were laminated, cylindrical shell sections in $[\pm 45_n/0_n]_s$ configurations, where n takes on values of 1, 2, and 3. The three structural parameters of radius, span, and thickness were varied according to a scaling relation and were chosen to represent approximate fuselage dimensions of general aviation and commercial transport aircraft. All specimens were evaluated for damage with dye-penetrant enhanced x radiography and sectioning after mechanical testing. The structural response changes both quantitatively and qualitatively for the different shell geometries and was categorized into three types based on the existence of the instability transition characteristics such as deformation shapes. The presence of the instability becomes more likely for deeper, thinner specimens where the ratio of membrane stiffness to bending stiffness is higher. This can be characterized by a structural parameter involving geometric and material factors. The majority of the specimens showed no damage, but the limited experimental evidence did show plate-like damage occurring in the shell specimens before any instability. Suggestions for further work to extend these findings are made.

I. Introduction

THE performance of composite structures during low-velocity impact events is an important design consideration for aerospace structures. The low through-thickness strength characteristics of laminated composites make them particularly vulnerable to out-of-plane loadings such as transverse impact events. Considerable research has, therefore, been devoted in recent years to understanding the impact response, including damage resistance and damage tolerance, of composite structures.[1–3] However, the majority of the work has been on laminated plates, with far less consideration given to the damage resistance of composite shells.[4,5] Because many aerospace structural components, such as fuselage panels, are shells and not plates, the current knowledge gained from research on the impact of plates may not apply to all structural configurations. To establish a comprehensive understanding of the transverse impact of general aerospace structures, it is, therefore, necessary to study the structural behavior and the related damage resistance characteristics of composite shells.

More specifically, there is a need to recognize and study the unique characteristics of shells as compared to plates. Differences in geometric coupling between bending and membrane deformations for plates and shells can cause significant changes in the structural response. A transversely loaded plate will develop tensile membrane stresses as the deflections increase, thus, giving a monotonically stiffening and stable force-deflection response. A convex shell, however, instantly generates compressive membrane stresses under transverse load, which may result in an instability as the force-deflection response moves between two stable equilibrium paths.[6–10] This can involve either limit-point or bifurcation buckling. A recent study has shown that this instability can dramatically improve the energy absorption characteristics of the structure and is also important in the determination of the equivalence of plate and shell damage states based on peak force.[10] The existence of asymmetric deformation shapes within the instability region has been reported for arches and cylindrical panels subjected to line loads.[6,11–13] However, relationships between the deformation shapes and the instability in the force-deflection response of a typical engineering laminate, that is, one with bending-twisting coupling subjected to the point-load condition, often experienced during foreign object impact, have not been explored. Furthermore, experimental results for the deformation shapes of such panels are currently not available in the literature. To extend fully the existing knowledge of plate impact to include shells, the underlying mechanisms of this instability, including the complex deformation shapes, must first be understood.

The overall objective of the current work is to gain a more detailed understanding of the mechanisms associated with the snap-through instability and its influence on the structural response and damage development of shell panels representative of realistic fuselage configurations. This is accomplished by experimental investigation of the force-deflection response and the evolution of full-field deformation shapes. Static indentation tests are used to simulate large-mass, low-velocity (nonballistic) transverse impact conditions.[4,10,14–16]

II. Approach

An experimental investigation utilizing quasi-static loading conditions was carried out to gain a more detailed understanding of the structural response and damage characteristics of convex composite shells. The shells considered were cylindrical convex sections made from Hercules AS4/3501-6 prepreg tape in a $[\pm 45_n/0_n]_s$ configuration, where n takes on the values of 1, 2, and 3. This configuration was chosen for comparison with previous impact investigations[10,17–19] and to utilize the effective ply concept for damage comparison.[19] The ply angle is relative to the circumferential direction of the shell, as shown in Fig. 1.

Presented as Paper 98-1992 at the AIAA/ASME/ASCE/AHS/ASC 39th Structures, Structural Dynamics, and Materials Conference, Long Beach, CA, 20–23 April 1998; received 20 March 2002; revision received 28 August 2003; accepted for publication 30 January 2004.

*Graduate Student, Technology Laboratory for Advanced Composites, Department of Aeronautics and Astronautics; currently Research Aerospace Engineer, U.S. Air Force Materials Laboratory, 2941 P. Street, Wright–Patterson Air Force Base, OH 45433.

†Professor and MacVicar Faculty Fellow, Technology Laboratory for Advanced Composites, Department of Aeronautics and Astronautics. Associate Fellow AIAA.

‡Boeing Assistant Professor, Technology Laboratory for Advanced Composites, Department of Aeronautics and Astronautics. Member AIAA.

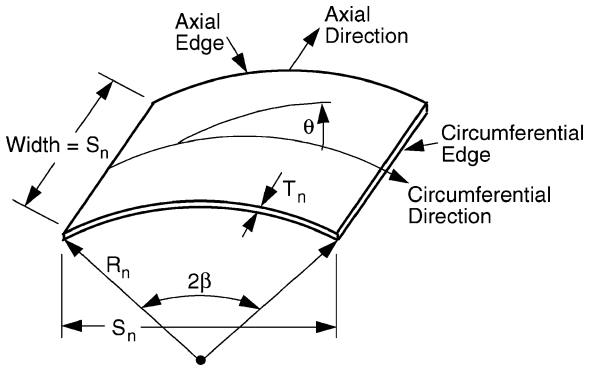

Fig. 1 Generic test specimen with geometric variables R_n (radius), S_n (span), and T_n (thickness).

Each of the three structural parameters radius R, span S, and thickness T, as defined in Fig. 1, was varied according to the following scaling relation:

$$X_n = n(X_1) \tag{1}$$

where X represents any of the three structural parameters, X_1 represents the base value for structural parameter X, and n takes on various values. The base values of the structural parameters R_1 (152 mm), S_1 (102 mm), and T_1 (0.804 mm) have been established in previous work[4,17] and were followed in this investigation. Radius parameters of R_6 and R_{12} with values of 914 mm (36 in.) and 1829 mm (72 in.) were chosen to represent approximate fuselage dimensions of general aviation and commercial transport aircraft, respectively.[20] Span parameters of S_1, S_2, and S_3 with values of 102, 203, and 305 mm and thickness parameters of T_1, T_2, and T_3 with values of 0.804, 1.608, and 2.412 mm were chosen to encompass typical stringer spacings and thicknesses found in commercial aircraft.[20] As noted earlier, the chosen layup allows for thickness scaling via the effective ply concept, that is, the effective thickness of material at each unique angle is changed in the same ratio, thereby keeping the number of ply mismatch interfaces constant.[21] This eliminates any influence on the damage state due to a changing number of ply mismatch interfaces and allows the effects of the structural parameters on the damage to be more clearly evaluated.

All possible combinations of geometric parameters were tested, thereby giving a fully populated test matrix. The total number of specimens tested for each geometry was dependent on the damage characteristics, with a minimum of one test for each geometry to measure deformation shapes.

The force-deflection response and damage characteristics of convex shells have been shown to be equivalent for quasi-static loading and low-velocity/large-mass impact conditions.[4,10,16–17] Static tests are desirable because they are easier to conduct and standardize due to the elimination of impact-related variables.[15] Quasi-static testing was, therefore, utilized in the present investigation to simulate low-velocity/large-mass impact conditions.

The portion of the response where compressive membrane stresses develop in the circumferential direction, including a possible instability region, is of particular interest because this has been identified as the primary difference from plate behavior.[6,9,10] The experimental tests were, therefore, designed to capture only the portion of the response with compressive membrane loading. The transition from compressive to tensile membrane loading was assumed to be complete when the convex panel reached a fully inverted, or concave, configuration. This criterion was used to terminate each test.

A quasi-static test was performed for each combination of geometric parameters. Contact force at the loading point and deflection data on the panel surface were recorded. All tested specimens were subsequently evaluated for damage by the use of dye-enhanced x radiography and sectioning. Additional tests were performed on specimens types that exhibited damage to further investigate damage incipience and development.

III. Experimental Techniques

An overview of the experimental procedures is given in this section. A more detailed description of all procedures can be found in Ref. 22.

A. Specimen Preparation

Laminates measuring 305 mm (12 in.) × 349 mm (14 in.) were laid up by hand and subsequently placed on cylindrical molds and cured with the standard manufacturer's cure cycle with full vacuum and 0.59-MPa external pressure throughout the 1-h flow stage at 116°C and 2-h set stage at 177°C of the autoclave cure.[22,23] Each laminate was also subjected to an 8-h postcure at 177°C. The laminates were held in special shell fixtures and trimmed with a water-cooled diamond saw to remove resin-rich edges and were then cut to the appropriate specimen sizes. The resulting variations in specimen thickness and radii were determined, with special mapping techniques, to be less than 8% (Ref. 22).

B. Testing

The specimens were placed in a test fixture (Fig. 2) designed specifically for the transverse loading of cylindrical shells.[17,22] Pinned/no in-plane sliding, that is, hinged, boundary conditions along the circumferential edges and free boundary conditions along the axial edges were approximated by the test fixture. Hinged circumferential edges restrict in-plane motion, thereby generating the compressive membrane stresses necessary to produce an instability, whereas free axial edges allow full panel rotation, which enhances the global deformations. The circumferential edges rest against the supports in shallow grooves that minimize the resistance to rotation inevitably created by friction. Note that the rotation condition provided by an actual stringer support falls somewhere between simply supported and clamped conditions.

Deformation shapes of each specimen were obtained in situ by a deflection measurement assembly mounted to the base of the test fixture. The assembly consists of a noncontact laser displacement transducer, with a resolution of 10 μm, mounted to a moveable traverse mechanism. The traverse provides continuous movement in the spanwise direction at discretely spaced axial intervals of 12.7 mm. With a suitable traversing speed and data sampling rate, detailed spanwise deformation shapes are traced out from below the shell at five predetermined axial positions by the laser. This allows the full-field deformation shapes of the entire panel to be inferred readily.

Quasi-static tests were conducted on an MTS-810 uniaxial testing machine under stroke (deflection) control. The resolution of stroke control varies from 6.2 to 31.0 μm, depending on the choice of stroke range. The test fixture, with the specimen in place, is mounted to the machine's lower grip, whereas the 12.7-mm hemispherical steel indentor and MTS 8896 N (2000-lb) load cell, with a maximum resolution of 0.66 N, are mounted in series to the fixed upper grip. Each test consists of an application of forward stroke until the shell reaches an approximately concave configuration, followed by reverse stroke back to the original unloaded position. The stroke rate

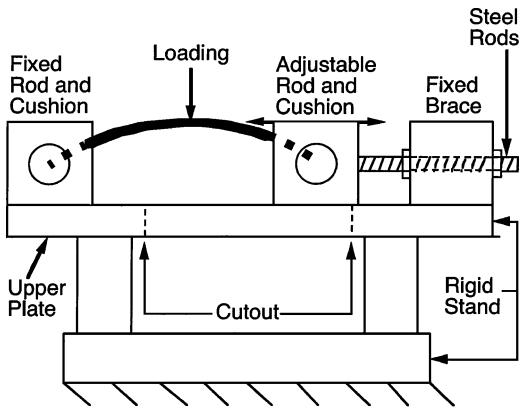

Fig. 2 Side view of test fixture with convex shell.

is set such that the total uninterrupted application of forward and reverse stroke takes 12 min. Subsequent procedures differ based on whether the test is for the purpose of deformation shape or damage measurement.

The first set of tests performed were to obtain the deformation shapes throughout the snap-through process. Tests are carried out up to the point where the originally convex panel assumes a fully inverted, that is, concave, configuration, which typically occurs as the deflection value reaches twice the original specimen height. During each test, the application of a forward stroke is interrupted and held at 10 equally spaced intervals of center deflection during which deformation shape data are taken. This yields a full-field deformation shape evolution for each specimen with increasing center deflection.

Separate data acquisition systems were utilized during each test due to the different sampling frequency requirements of the various measurements. Load and stroke data are sampled directly from the MTS electronic outputs at 0.5 Hz continuously throughout the test by the use of Labview data acquisition software. The deformation shape data from the traverse assembly and laser are taken only during the held-stroke portions of the tests and are each sampled at 20 Hz with a Nicolet 206 digital oscilloscope. The speed of the traverse is adjusted for each specimen to yield approximately 100 data points for each spanwise deformation shape. Practical limitations on the size of data files and test duration necessitated such an arrangement.

Additional quasi-static tests were performed to further investigate damage incipience and development in specimen geometries that showed damage in the first test, that is, when deformed into the fully inverted configuration. These subsequent damage tests were conducted in an effort to identify damage incipience and development with respect to the primary force-deflection regimes as defined in Fig. 3: first equilibrium path, instability region, and second equilibrium path. Separate tests were conducted up to center-deflection values corresponding to the local extremum that separates the primary regimes. This allowed the regime that contained the point of damage incipience to be identified. One additional test was then conducted in an attempt to identify the damage incipience point more closely and to further clarify the overall development of damage with increased loading. Specimen geometries that showed no signs of damage in the deformation-shape tests would have damage incipience and development occurring further along the second equilibrium path where tensile membrane stresses develop. As mentioned earlier, this was beyond the limits imposed by the design of the grooved-edge boundary conditions. Furthermore, damage characteristics for these specimen geometries are similar to those found in plates[9,16] and are not the focus of this study.

C. Damage Evaluation

All specimens were inspected for damage by the use of dye-penetrant enhanced x radiography and sectioning. Dye penetrant was injected into a 0.79-mm hole drilled at the contact point. Flash tape was placed on the back surface of the panel to contain the low-viscosity dye, which easily wicks into the damaged regions via capillary action. The damaged regions show up as dark regions in an x ray photograph. This technique provides a through-thickness integrated view of damage, including matrix splits and delaminations. After the x radiography was completed for a specimen that revealed some damage, the specimen was sectioned along the center span with a diamond saw. The cut surface was buffed with a felt bob rotating in a drill press while a slurry mixture of powder and water was applied. This created the smooth surface necessary to identify the damaged areas when viewed with an optical microscope at 30× magnification. Transverse matrix cracks and delaminations are observed as white lines against the black surface of the material. This technique allows the distribution of damage through the thickness to be identified at all locations along the center span.

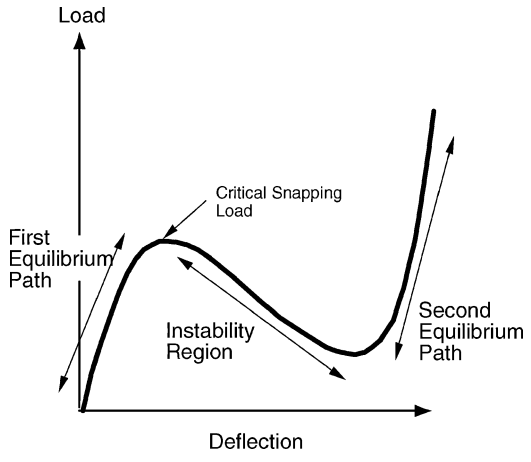

Fig. 3 Illustration of load-deflection response of convex shell with instability.

IV. Results and Discussion

The instability in the force-deflection response of a convex shell, under stroke-controlled conditions such as a low-velocity impact event,[11] is shown in Fig. 3. The response begins on the first equilibrium path of nonlinear prebuckling, characterized by its softening behavior as it approaches a local maximum termed the critical snapping load. Beyond this point, in postbuckling, the response moves into the instability region, characterized by its negative slope. The response then proceeds through a local minimum and onto the second equilibrium path, which exhibits monotonic stiffening behavior. An important distinction to be made regarding this force-deflection response is that this instability region can only exist under stroke-controlled conditions. If the response is load controlled, the panel will dynamically snap through to an equal load on the second equilibrium path, which corresponds to an inverted concave configuration. This investigation only considers the buckling phenomenon as manifested under the stroke-controlled conditions of a low-velocity impact event. In fact, there is a possibility that the panel could dynamically snap-through to the inverted configuration even when stroke-controlled conditions are utilized. If the force-deflection response crosses the zero-force axis, this indicates that a tensile force would have to be applied by the indentor to maintain contact with the panel under further deformation. Because a negative force could not occur with the simple indentor used in the experiments, this zero-crossing point, therefore, coincides with the panel dynamically snapping away from the indentor into the inverted configuration. Also note that some convex shells do not display an instability region and simply transition from the first to second equilibrium paths via an inflection point. The general shell response is, however, in contrast to the plate response, which is entirely stable and monotonically stiffening.

The deformation shape evolutions recorded by the laser-traverse assembly provide a snapshot of the panel's shape at successive states of deformation. However, for this paper, a more compact presentation of the data is achieved by considering only what happens along the central spanwise and axial sections of the panel. Close examination of the full data sets show that the primary aspects of the deformation behavior are adequately represented by the data along these central sections. Deformation shape evolutions along these central sections are presented in the sections that follow. The full details of the deformation shapes can be found in Ref. 22.

A. Characterization of Response Types

Three distinct types of experimental load-deflection responses were observed and characterized: inflection (type 1), limit-point buckling (type 2), and bifurcation buckling (type 3). Although limit-point and bifurcation buckling both involve an instability, they are different in many respects.[24] Instability simply refers to a region of negative slope in the load-deflection response. In limit-point buckling, the prebuckling state grows nonlinearly (and smoothly) to the critical point, which is characterized by zero slope. In contrast, the change in slope in bifurcation at the bifurcation point can be discontinuous because bifurcation involves a change in mode shapes and, thus, a switching (or branching) to a secondary equilibrium path. Therefore, both the load-deflection responses and the mode

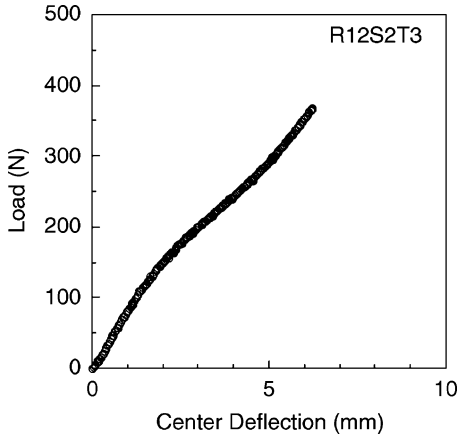

Fig. 4 Force-deflection response for specimen $R_{12}S_2T_3$, showing type 1 behavior.

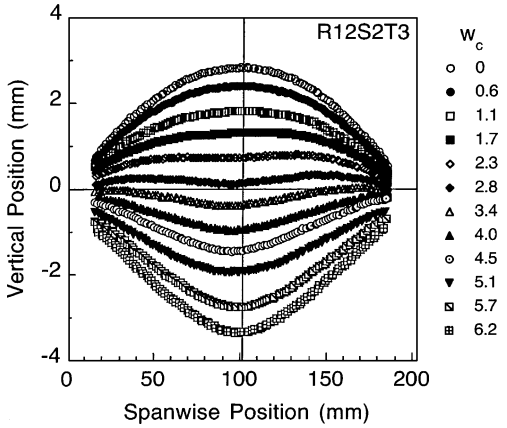

Fig. 5 Central spanwise deformation-shape evolution for specimen $R_{12}S_2T_3$ at different values of center deflection w_c.

shapes were considered when the response types were categorized. Type 1 responses are found to be smooth and stable, with no instability. Response types 2 and 3 both have regions of instability, that is, they buckle although each has a different buckling mechanism and associated deformation characteristics: Type 2 cases are observed to have smooth transitions through the instability region and no changes in mode shapes, whereas type 3 cases oftentimes have nonsmooth regions and always have changes in mode shapes.

As noted, type 1 load-deflection responses were entirely stable and transition from the first to second equilibrium paths via an inflection point rather than an instability region, as shown in Fig. 4. The experimental deformation shapes along the central spanwise and axial sections, for type 1 specimens, were fully symmetric about the loading point. A typical type 1 central spanwise deformation-shape evolution, given in Fig. 5 at different values of center deflection w_c, clearly shows the progression from a convex to a concave configuration. Inflection points, located symmetrically about the loading point, can be seen to grow steadily outward toward the boundary as the center deflection is increased. The central axial deformation shape evolution for the same specimen, given in Fig. 6, shows deformations that are approximately uniform throughout the test, although there is some axial variation at larger center deflections symmetric with the loading point. The progression of deformation mechanisms in the spanwise direction are, therefore, similar at all axial points for these specimens, yielding a shape with very little variation in the axial direction.

Specimens with an experimental type 2 force-deflection response smoothly transition between equilibrium paths via an instability region, as seen for a representative specimen, $R_{12}S_3T_3$, in Fig. 7. The small deviations from a smooth response on the underside of the curve are due to small changes in load experienced during the held-stroke positions and are not considered significant.

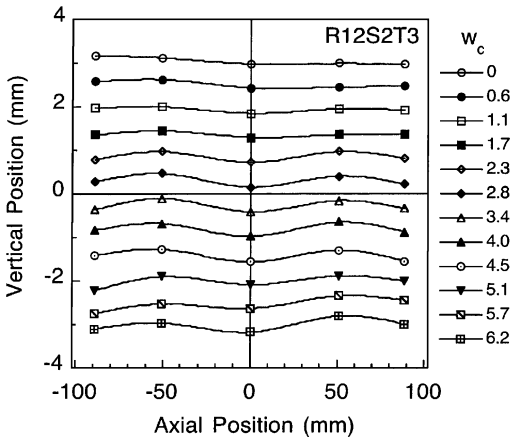

Fig. 6 Central axial deformation-shape evolution for specimen $R_{12}S_2T_3$ at different values of center deflection w_c.

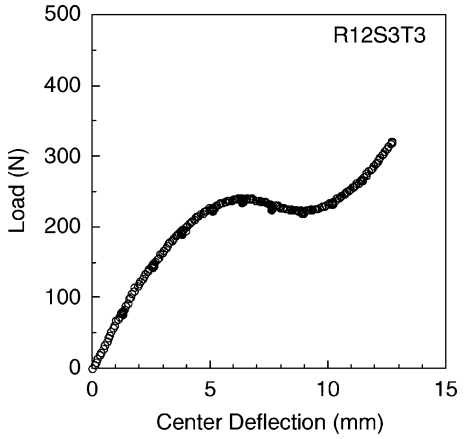

Fig. 7 Force-deflection response for specimen $R_{12}S_3T_3$, showing type 2 behavior.

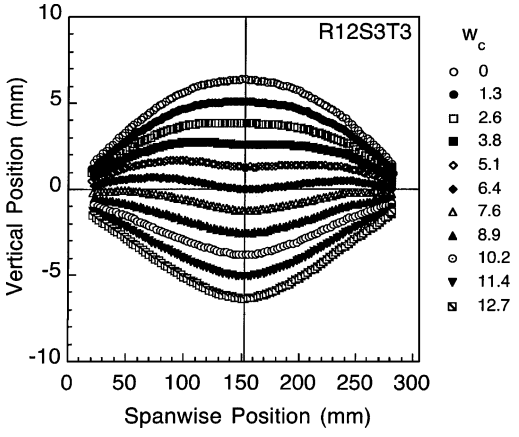

Fig. 8 Central spanwise deformation-shape evolution for specimen $R_{12}S_3T_3$ at different values of center deflection w_c.

The deformation shapes for type 2 specimens along the central sections displayed fully symmetric behavior, as seen for specimen $R_{12}S_3T_3$ in Figs. 8 and 9. Observations similar to those made for the central spanwise evolutions of type 1 specimens apply here as well. The central axial deformation shape evolutions of Fig. 9 show that a concave shape initially develops with the maximum deflection at the center beneath the loading point, that is, at 1.3 mm. As the center deflection is increased to larger values, such as 8.9 mm, the shape becomes flatter, which is similar to the type 1 specimens. The key difference in the response of type 1 and 2 specimens is that the latter shows a limit-point behavior in the load-deflection data.

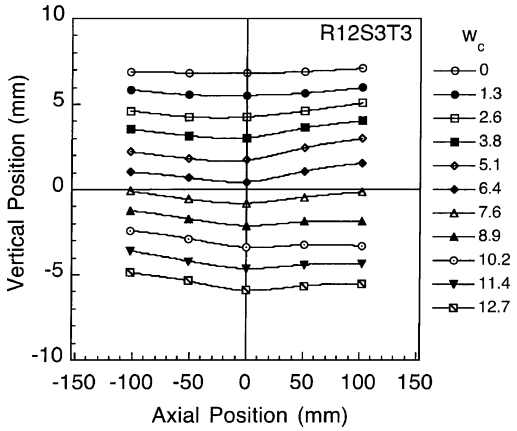

Fig. 9 Central axial deformation-shape evolution for specimen $R_{12}S_3T_3$ at different values of center deflection w_c.

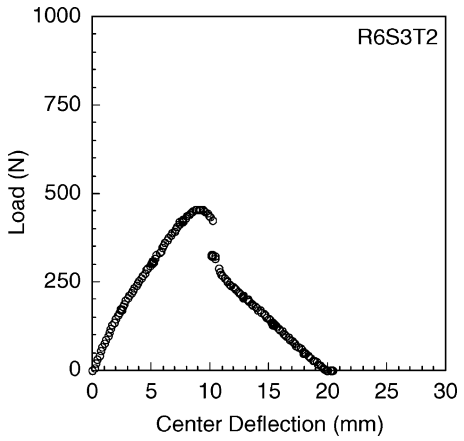

Fig. 10 Force-deflection response for specimen $R_6S_3T_2$, showing type 3 behavior.

Type 3 force-deflection responses often showed nonsmooth behavior along with a zero-force crossing as the panel snapped away from the indentor into an inverted configuration. As shown in Fig. 10 for specimen $R_6S_3T_2$, there is a discontinuity, or load-drop, at the beginning of the instability region, followed by a zero-force crossing further along the instability region. Such type 3 specimens, therefore, dynamically snapped away from the indentor into the inverted configuration.

Deformation shapes for type 3 specimens were symmetric on the first equilibrium path and became asymmetric at some point near the critical point within the instability region. The asymmetric shapes can be seen for specimen $R_6S_3T_2$ in the central spanwise and axial deformation shape evolutions shown in Figs. 11 and 12. The central spanwise deformation shapes develop a sinusoidal shape whereas the central axial deformation shapes become slanted to one side. The axial slanting noted in these cases is attributed to bending–twisting coupling in this laminate type. The nearly sinusoidal shape of the shell after bifurcation (Fig. 11) implies that the left-hand side of the shell undergoes significantly more bending than the right-hand side. Increased twisting is, thereby, expected on the left-hand side as compared to the right-hand side. This twisting response is manifested as the slanting noted in the axial variation in Fig. 12. The symmetric nature of the inverted (concave) shell mode at the center deflection of 24.8 mm in Fig. 11, and the lack of slanting in the corresponding axial shape in Fig. 12, further supports this explanation. Panel snap away can be detected in Figs. 11 and 12 by an inconsistently large interval of center deflection as the inverted configuration is attained. Note that a fully symmetric deformation shape is recovered, along both the central spanwise and axial sections, after the panel snaps into the inverted configuration.

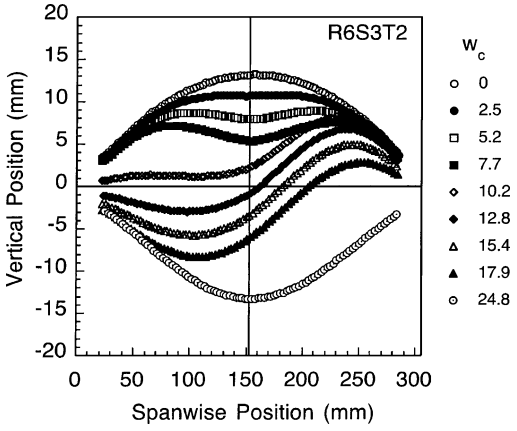

Fig. 11 Central spanwise deformation-shape evolution for specimen $R_6S_3T_2$ at different values of center deflection w_c.

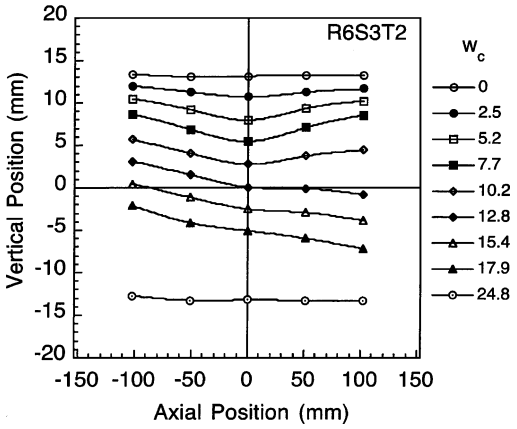

Fig. 12 Central axial deformation-shape evolution for specimen $R_6S_3T_2$ at different values of center deflection w_c.

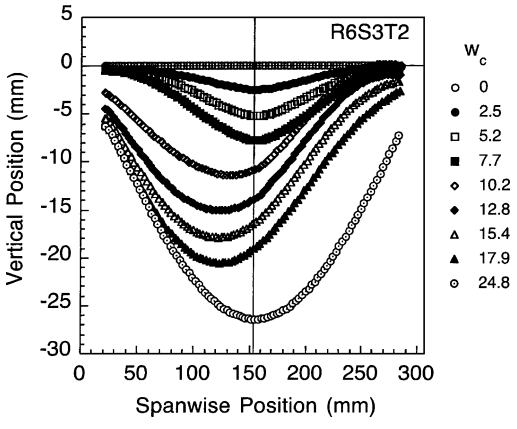

Fig. 13 Central spanwise deflection-from-undeformed evolution for specimen $R_6S_3T_2$ at different values of center deflection w_c.

B. Effect of Structural Parameters

Parameters that characterize the structural behavior in the experiments are utilized to demonstrate relationships between the symmetry of deformation shapes, load-deflection behavior, and the initial geometric configuration.

The state of symmetry for the deformation shapes along the central span is further quantified by consideration of the deformations relative to the initial configuration, or the deflection-from-undeformed shapes. These shapes are generated by subtraction of the initial configuration from all deformation shapes, as shown for specimen $R_6S_3T_2$ in Fig. 13. Symmetric deformation shapes have a maximum deflection at the midspan, whereas asymmetric deformation

Table 1 Values of the parameter λ and response type[a]

	T_1		T_2		T_3	
Span	R_6	R_{12}	R_6	R_{12}	R_6	R_{12}
S_1	4.04/2	3.00/1	2.82/1	1.97/1	2.32/1	1.63/1
S_2	7.79/3	5.87/3	5.75/3	4.27/2	4.53/2	3.29/1
S_3	11.8/3	8.51/3	8.46/3	6.14/3	6.87/3	4.96/2

[a]λ-Value/response type.

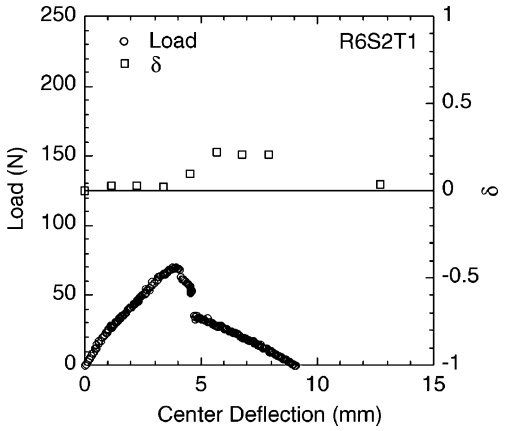

Fig. 14 Force-deflection and δ-deflection responses of specimen $R_6S_2T_1$ (type 3).

shapes show a migration of the point of maximum deflection away from the midspan. Thus, a degree-of-asymmetry parameter δ is defined as the distance the point of maximum deflection migrates away from the midspan location, normalized by the panel halfspan. Note that transversely loaded plates always have a maximum deflection and, hence, maximum curvature, at the loading point, that is, $\delta = 0$. However, convex shells that exhibit asymmetric shapes may have their maximum deflection, curvature, and bending stresses away from the loading point.

The value of δ remains near zero throughout the test for type 1 and 2 specimens because they exhibit fully symmetric deformation shapes. However, type 3 specimens, such as $R_6S_2T_1$, develop nonzero δ values after the load drop in the force-deflection diagram, as seen in Fig. 14, suggesting that the load drop is directly related to the onset of asymmetric deformation shapes and, thus, bifurcation.

Characterization of response type based solely on structural configuration and layup were also investigated. Previous analytical work[6] with line-loaded orthotropic shells yields a geometric/material parameter λ that governs the response type:

$$\lambda = A_{11}R^2\beta^4 \big/ D_{11} \tag{2}$$

where A_{11} and D_{11} are the components of the laminate in-plane and bending stiffness matrices in the circumferential direction, R is the radius of curvature, and β is one-half of the included angle, as shown in Fig. 1:

$$\beta = \sin^{-1}(S/2R) \tag{3}$$

where S is the shell span. The nonlinear analysis assumes moderately large rotations and no variation in the width of the shell (as in an arch). For laminates with effective plies, this parameter varies with the panel height-to-thickness ratio. Thin, deep shells have higher values of λ, whereas shallow, thick panels have lower values. The three response types are then defined by different ranges of λ. Response types and λ values are given in Table 1. As with earlier work, the same variation of response type with the λ parameter is observed in this work. Shells with values of λ less than 3.5 have an inflection point (type 1), those with values of λ between 3.5 and 5.0 experience a limit point (type 2), and those with values of λ greater than 5.0 bifurcate (type 3). In addition, there is a further subclass

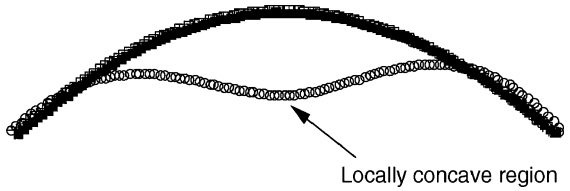

Fig. 15 Exploded view of spanwise deformation near critical snapping displacement for specimen $R_6S_3T_3$: ■, undeformed and ○, near critical snapping displacement.

within type 3. Three specimens ($R_6S_2T_2$, $R_6S_3T_3$, and $R_{12}S_3T_2$) had a smooth instability region, whereas the other five type 3 specimens all had nonsmooth instability behavior (Fig. 10). These three noted specimens had the lowest values of λ within the type 3 specimens, except for the case of specimen $R_{12}S_2T_1$.

As expected, these ranges of λ do not precisely correspond to those derived analytically. The disagreement is due to material couplings (e.g., bend–twist), the assumption of line-load, and/or deviations from the idealized boundary conditions of the model. However, the parameter adequately captures and groups the type of specimen response for all specimens tested.

C. Damage Response

Only the thickest and deepest specimen ($R_6S_3T_3$, which had type 3 behavior) revealed damage when investigated with x-ray and sectioning techniques. As a result, the damage testing program was carried out only for this specimen geometry. Further tests conducted up to center deflections within each key regime revealed that this specimen damaged very near the critical snapping load and before entering the instability region. Incipient damage was identified as a matrix crack on the backface of the panel just below the loading point along the +45-deg direction in the 45-deg ply. The damage progression showed the development of delaminations at the interface with the −45-deg ply group with increasing center deflection. This damage behavior is very similar to the incipient tensile failure and subsequent ply mismatch delamination seen in transversely loaded composite plates.[1,3] A possible explanation for this behavior is that the tensile component of the bending stress dominates the compressive membrane stresses as the critical snapping load is approached. An exploded view of the central spanwise deformation shape very near the critical snapping load, shown in Fig. 15, shows that there is a locally concave region of large curvature near the loading point. This configuration would support the existence of high local bending stresses and, thus, the tensile failure observed in the experiments. Panel deformation shapes at earlier stages of the first equilibrium path showed much smaller bending deformations beneath the loading point. Therefore, specimens whose damage incipience occurs at this early stage may show different damage behavior due to the predominantly compressive membrane conditions.[25,26] Further work to investigate the detailed state of stress is recommended to verify this interpretation.

Damage incipience and growth for most specimen geometries in this investigation were not found to occur within the regimes of compressive membrane stresses. Therefore, any conditions that would induce damage in these specimens would occur on the second equilibrium path under predominantly tensile membrane stresses and would, therefore, likely have characteristics similar to plates.[10]

V. Implications for Damage Resistance

The results of the current work tend to confirm the use of peak force as a critical damage metric for these convex shells. The peak force and damage state of specimen $R_6S_3T_3$, at progressive states of deformation beyond the critical snapping deflection, showed very little variation, even though the center deflection varied by as much as 47%. This suggests that peak force is a controlling parameter in the damage response, even with the presence of an instability. This $R_6S_3T_3$ specimen has platelike damage characteristics that occurred on the first equilibrium path. This behavior most likely results when incipient damage occurs near the onset of buckling, that is, near

the critical snapping load, where the bending stresses can become dominant. Further investigation into the similarities between shell and plate damage characteristics in this regime, including the use of peak force as a damage metric, is warranted.

The majority of the specimens in this investigation show the ability to be deformed into the fully inverted configuration without sustaining damage. This suggests that the damage initiation and development on further loading would likely be dominated by tensile membrane loading and, therefore, be very similar to that observed for plates. However, before a complete extension can be made to actual fuselage structures, the support along the circumferential edges must also be considered.

The peak impact force reached during an impact event depends strongly on the qualitative nature or type of force-deflection response exhibited by the shell. The consistent trends in the force-deflection response type with geometric/material parameters demonstrates how a shell structure can be designed to have markedly different characteristics. Previous work has shown that the instability provides increased impact energy absorption through smaller contact forces.[10] When appropriate, this characteristic of the response could be exploited to design a more damage-resistant structure. The simple parameter λ can be used as a preliminary means to assess the response of a given shell structure, including the possible presence of an instability and asymmetric deformation shapes. In addition, the asymmetric deformation shapes that occur during bifurcation buckling (type 3 response) may affect the damage characteristics. Asymmetric deformation shapes allow the possibility of high bending stresses and, hence, possible damage formation, away from the loading point. In such cases, evaluation of the damage with the common laboratory method of dye-penetrant enhanced x radiography at the loading point would be inappropriate.

VI. Summary

The structural mechanisms of transversely loaded convex shells have been investigated experimentally. The structural response changes both quantitatively and qualitatively for different shells and is characterized into three types in this work. The presence of an instability in the force-deflection response becomes more likely for deeper, thinner specimens, where the ratio of membrane stiffness to bending stiffness is higher, as characterized by the structural parameter λ. Specimens with very high values of this parameter develop asymmetric deformation shapes and snap away from the indentor into the inverted configuration at some point within the instability region. The transition from symmetric to asymmetric deformation shapes and the panel snap-away phenomenon are dynamic processes that exist even under quasi-static, stroke-controlled loading where the indentor is not attached to the specimen.

The structural response is inextricably related to the damage characteristics of the shell. Previous work has shown that shells with type 1 or type 2 responses exhibit platelike damage behavior when incipient damage occurs on the second equilibrium path. Limited experimental evidence in this study shows that plate-like damage, that is, tensile failure on the back face at the loading point, can also occur at points on the first equilibrium path due to large bending deformations near the loading point. The interplay between bending and membrane stresses at points along the first equilibrium path warrants further examination. Shells that have an instability and also develop asymmetric deformation shapes (type 3 bifurcation response) could conceivably develop damage away from the contact point because this is no longer the point of maximum curvature. Changes in stress distributions and elastic behavior for the different structural response types and regimes are, therefore, crucial to the development and design of damage resistant composite shell structures.

The different types of structural behavior exhibited by convex composite shells have been shown to depend on both the panel geometry and material. Although a line-load parameter was shown to characterize the trends for the shells of square planform in this investigation, the role of different boundary conditions including support along the axial edges, should be studied in more detail because actual fuselage panels possess some degree of rotational restraint along both the axial and circumferential edges. The effect of a varying planform will also enter into this consideration. The role that specimen geometry and boundary conditions play in generating the membrane and bending components of stress should be examined further through analysis. In addition, the limit-point and bifurcation buckling behaviors should be examined analytically, including the effects of imperfections, because markedly different responses and deformation shapes can develop. With a fundamental understanding of the full-field stress state and its relation to the global structural behavior and damage formation, intelligent use can be made of composites in the design of damage resistant fuselage structures.

Acknowledgment

This work was sponsored by the Federal Aviation Administration under Research Grant 94-G-037.

References

[1]Abrate, S., "Impact on Laminated Composite Materials," *Composites*, Vol. 24, No. 3, 1991, pp. 77–99.

[2]Abrate, S., "Impact on Laminated Composites: Recent Advances," *Applied Mechanics Review*, Vol. 47, No. 11, 1994, pp. 517–544.

[3]Cantwell, W. J., and Morton, J., "The Impact Resistance of Composite Materials," *Composites*, Vol. 22, No. 5, 1991, pp. 55–97.

[4]Wardle, B., and Lagace, P., "Behavior of Composite Shells Under Transverse Impact and Quasi-Static Loading," *AIAA Journal*, Vol. 36, No. 6, 1998, pp. 1065–1073.

[5]Krishnamurthy, K. S., Mahajan, P., and Mittal, R. K., "A Parametric Study of the Impact Response and Damage of Laminated Cylindrical Composite Shells," *Composites Science and Technology*, Vol. 61, 2001, pp. 1655–1669.

[6]Johnson, E. R., Hyer, M. W., and Carper, D. M., "Response of Composite Material Shallow Arch to Concentrated Load," *Journal of Aircraft*, Vol. 23, No. 6, 1986, pp. 529–536.

[7]Marshall, I. H., Rhodes, J., and Banks, W. M., "Experimental Snap-buckling Behaviour of Thin GRP Curved Panels Under Lateral Loading," *Composites*, Vol. 8, No. 2, 1977, pp. 81–86.

[8]Marshall, I. H., Rhodes, J., and Banks, W. M., "The Nonlinear Behaviour of Thin, Orthotropic, Curved Panels Under Lateral Loading," *Journal of Mechanical Engineering Science*, Vol. 19, No. 1, 1977, pp. 30–37.

[9]Marshall, I. H., and Rhodes, J., "Snap-Buckling of Thin Shells of Rectangular Planform," *Stability Problems in Engineering Structures and Components*, edited by T. H. Richards and P. Stanley, Applied Science, London, 1979, pp. 249–264.

[10]Wardle, B. L., and Lagace, P. A., "Importance of Instability in the Impact Response of Composite Shells," *AIAA Journal*, Vol. 35, No. 2, 1997, pp. 389–396.

[11]Timoshenko, S., *Theory of Elastic Stability*, Engineering Societies Monographs, McGraw–Hill, New York, 1936, pp. 204–238.

[12]Schreyer, H. L., and Masur, E. F., "Buckling of Shallow Arches," *Journal of Engineering Mechanics*, Vol. 92, 1966, pp. 1–10.

[13]Fung, Y. C., and Kaplan, A., "Buckling of Low Arches or Curved Beams of Small Curvature," NACA TN 2840, Nov. 1952.

[14]Jackson, W. C., and Poe, C. C., Jr., "The Use of Impact Force as a Scale Parameter for the Impact Response of Composite Laminates," *Journal of Composites Technology and Research*, Vol. 15, No. 4, 1992, pp. 282–289.

[15]Lagace, P. A., Williamson, J. E., Tsang, P. H. W., Wolf, E., and Thomas, S., "A Preliminary Proposition for a Test Method to Measure (Impact) Damage Resistance," *Journal of Reinforced Plastics and Composites*, Vol. 12, No. 5, 1993, pp. 584–601.

[16]Wardle, B. L., and Lagace, P. A., "On the Use of Quasi-Static Testing to Assess Impact Damage Resistance of Composite Shells," *Mechanics of Composite Materials and Structures*, Vol. 5, No. 1, 1998, pp. 103–121.

[17]Wardle, B. L., "Impact and Quasi-Static Response of Cylindrical Composite Shells," Technology Lab. for Advanced Composites, TELAC Rept. 95-4, S. M. Thesis, Dept. of Aeronautic and Astronautics, Massachusetts Inst. of Technology, Cambridge, MA, May 1995.

[18]Lagace, P. A., and Wolf, E., "Impact Damage Resistance of Several Laminated Material Systems," *AIAA Journal*, Vol. 33, No. 6, 1995, pp. 1106–1113.

[19]Thomas, S., "Effects of Structural Parameters on the Static Indentation and Bending Behavior of Graphite/Epoxy Laminates," Technology Lab. for Advanced Composites, TELAC Rept. 93-9, S. M. Thesis, Dept. of Aeronautics and Astronautics, Massachusetts Inst. of Technology, Cambridge, MA, Sept. 1993.

[20]Niu, M. C. Y., *Airframe Structural Design—Practical Design Information and Data on Aircraft Structures*, 8th ed., Conmilit Press, Los Angeles, 1995, pp. 384–389.

[21]Lagace, P. A., Brewer, J. C., and Kassapoglou, C., "The Effect of Thickness on Interlaminar Stresses and Delamination," *Journal of Composites Technology and Research*, Vol. 9, Fall 1986, pp. 81–87.

[22]Tudela, M. A., "Structural Response and Damage Development of Cylindrical Composite Panels," TELAC Rept. 96-11, S.M. Thesis, Dept. of Aeronautics and Astronautics, Massachusetts Inst. of Technology, Cambridge, MA, Sept. 1996.

[23]Lagace, P. A., Brewer, J. C., and Varnerin, C., "TELAC Manufacturing Course Notes," Technology Lab. for Advanced Composites, TELAC Rept. 88-4B, Dept. of Aeronautics and Astronautics, Massachusetts Inst. of Technology, Cambridge, MA, Sept. 1991.

[24]Bushnell, K., *Computerized Buckling Analysis of Shells*, Mechanics of Elastic Stability, edited by H. H. E. Leipholz and G. Æ. Oravas, Vol. 9, Martinus Nijhoff, Dordrecht, The Netherlands, 1985, pp. 1–28.

[25]Cairns, D. S., Minguet, P.-A., and Abdallab, A. G., "Theoretical and Experimental Response of Composite Laminates with Delaminations Loaded in Compression," AIAA Paper 92-2223, April 1992.

[26]Whitcomb, J. D., "Mechanics of Instability-related Delamination Growth," NASA TM-100622, May 1988.

E. R. Johnson
Associate Editor